# Multidimensional Configuration-Space Models of the Electronic Factor in Electron Transfer by Superexchange: Implications for Models of Biological Electron Transfer

**M. C. Wells and R. R. Lucchese***

*Department of Chemistry, Texas A & M University, College Station, Texas 77843-3255*

*Received: April 26, 1999; In Final Form: July 7, 1999*

We employ multidimensional configuration-space models to investigate the electronic factor that appears in theories of electron transfer. Of particular interest is the electronic factor in models of long-range biological electron transfer (ET), which is thought to occur via a bridge-mediated superexchange mechanism. The configuration-space electron tunneling fluxes that we calculate give explicit information on the relative importance of many-electron effects such as correlation and hole vs particle transfer. The results from our models lead to a nonintuitive indication that simple state-space perturbation theory expressions for the electronic factor can lead to incorrect interpretations of electron-transfer processes. In particular, we find that the exclusion of lower-energy bridge bound states may misrepresent the bridge attractive potential and may result in significant errors in the electronic factor contribution to the electron-transfer rate. The importance of the lower energy bridge levels in describing the tunneling state does not, however, imply that hole transfer is important. We find that through-bond electron tunneling interactions are more reliably viewed in terms of the tunneling barrier (using WKB theory) than in terms of the energy gaps between the tunneling electron and the respective bridge bound and virtual states (i.e., a second-order perturbation theory perspective). In the present superexchange models we find no instance in which hole transfer dominates the ET mechanism; however, as the energy level of a bridge eigenstate approaches that of the donor−acceptor, we find that multiple transfer pathways are simultaneously possible. Finally, results from these models suggest that the effects of electron−electron repulsion are small and relatively unimportant.

## I. Introduction

Despite recent efforts toward attaining accurate electron-transfer (ET) rate predictions for the photosynthetic reaction center (PRC) and analogous biological ET reactions, the precise manner in which many of these types of ETs occur is still not known.[1−9] Nonetheless, the prospect that new device and synthetic technologies can be developed for use in artificial photosynthesis and biocatalysis ensures that the drive for biological ET rate prediction will continue unabated.[10−17] For long-range biological ET reactions in which neither the donor nor acceptor are closely coupled to the facilitating bridge, i.e., a nonresonant process, it is generally agreed that ET occurs through a mechanism of superexchange.[1] This process is typically viewed as one in which the coupling between the donor and acceptor is not direct and in which the electronic orbitals of the donor and acceptor complexes do not overlap. The distances between redox centers in the PRC are large, up to ∼10−20 Å, a circumstance in which we would expect the probability for tunneling to be low for ET across empty space. In proteins, however, the molecular structure intervening between the donor and acceptor is comprised of a series of bridging atoms that in the standard picture is thought to provide a sequence of overlapping orbitals that give rise to coupling between the donor and acceptor complexes. Experimental observations suggest that there are a number of biological ET systems, including the PRC, that can be described in this fashion.[8] In such systems the ET rate is controlled in whole or part by the electronic properties of the protein scaffold, or bridge, intervening between ET donor and acceptor sites. The net effect of these electronic properties is typically distilled into a single ET tunneling matrix element, also called the electronic factor, the further understanding of which is the topic of this work.

Modeling the ET process is not only important from the standpoint of predicting which molecular structures will exhibit the desired ET rate but it is also important to understand how and why the process occurs. From a theoretical standpoint, ab initio methods provide the most accurate avenue for determining tunneling matrix elements. However, these calculations are often computationally untenable for systems in the $10^2+$ kDa size range of many proteins. Some efforts are underway to develop ab initio methods that can accommodate very large systems,[18] but most work on large systems to date has relied upon simplifying approximations to reduce the size or extent of the calculation.[5] Often these assumptions reduce the problem to a two-state or few-state one-electron model, reminiscent of one of the earliest models of superexchange, the McConnel model.[19] Also, many models employ the tight binding approximation in which each bridge site only has nonnegligible interactions with its nearest neighbor. Although modern ET models on biological systems, systems that necessitate the model being large, have progressed substantially since the McConnel model, the discrepancies still observed between experimental and theoretical long-range biological ET data indicate that there is significant room for improvement.[20−24] One possibility for scrutinizing ET models, a strategy we pursue here, is to see how conventional approaches used in large electronic factor models fare when applied to smaller systems for which analytic solutions exist.[25−27] Certainly, it is reasonable to infer that an approximation

* To whom correspondence should be addressed.

10.1021/jp9913620 CCC: $18.00 
Published on Web 08/24/1999

deleterious to accurate results for a small system will be less valid for a large system of much greater complexity, such as the PRC.

Another common feature in large biological ET models is the use of state-space descriptions, or valence atomic orbital (VAO) models, in which the tunneling electron is described mathematically, for instance, in terms of a linear combination of states. In these state-space descriptions the exact identification of the electron-transfer mechanism may not be transparent because this linear combination, or mixing of states, leads to ambiguity in identification of transfer pathways.[1,4,5,7] The desire for a more explicit, less ambiguous expression of transfer mechanism has been a motivating force in the development of pathway methods;[28−32] still, many of the pathway models are semiempirical in nature and have not yielded the kind of mechanistic information necessary for design of biomimetic ET complexes. Two new applications to address this need for mechanistic tracking are the use of electron-transfer contact maps[33] and tunneling currents,[34,35] both of which provide more detailed information than the conventional state-space picture from valence atomic orbital models.

Three of the ideas expressed above formed the basis for the current study: (1) the effect of simplifying approximations on a smaller model can be compared to the exact solution as a test of their validity; (2) smaller models provide a context from which to view and test methods applicable to larger models; (3) a spatially explicit perspective yields more useful mechanistic information about electron transfers. The electron-transfer model we describe below is a one- to many-electron configuration-space model. One important and novel aspect of this work compared to other work in the literature is that by combination of the configuration-space approach with the method of tunneling fluxes, the ET process may be explicitly described *and visualized* in terms of the electronic structure of the bridge; i.e., which electronic configurations of the bridge are important to the ET process. One issue that we have addressed in this way is the relative importance of particle vs hole transfer in the ET process. In previous often-cited papers on biological ET, the ET process is modeled by either particle or hole transfer.[31,36] The current results illustrate how a path multiplicity may arise in which particle, hole, and mixed-mode transfers may occur simultaneously. Here, we coin the terminology "mixed-mode" transfer to describe a transfer process that other ET literature to our knowledge does not address but that the visual nature of the current results illustrates to be important in some cases.

Two simplifying assumptions used in large biological ET models involve the use of one-electron models neglecting electron−electron correlation and the use of reduced state-spaces wherein some or many of the bridge electronic states are in some manner deemed unimportant to the ET process and not included in the model as a result.[5] This paper addresses both of these issues. With respect to one- vs many-electron models in the context of biological ET, several authors have made the case that a one-electron model is sufficient.[1,37,38] For three spatial dimensions, visualizing results from a two-electron model effectively requires six dimensions, a conceptually difficult prospect. Alternatively, by use of one spatial dimension, it is much easier to directly visualize how electron−electron correlation affects tunneling, and we provide an example of this in the results below. Although spatially one-dimensional models are not directly comparable with more realistic models that are spatially three-dimensional, there are nonetheless important ET processes that occur by tunneling and that are well represented by spatially one-dimensional models. In particular, Heifets et al. have modeled simple linear chains of atoms as quasi-one-dimensional systems.[39] The results that we discuss here indicate that a one-electron model is sufficient to determine the electronic factor contribution to the ET rate.

The other simplifying assumption we address here, how leaving some of the bridge electronic states out of the model affects the electronic factor portion of the ET rate, has thus far been employed in part as a way to make calculations on large biological systems more tenable, since the size of the system is directly related to the difficulty of modeling it. In a recent review of biological ET, Beratan and Onuchic[8] have commented that caution must be exercised in excluding selected states from models of ET systems. In this work we look at the effect of excluding selected states from the model and find that such a practice may often result in a calculated electronic factor and hence ET rate, which is too low. When examining the causative factors of this result, we find that the exclusion of certain states results in a misrepresentation of the attractive nature of the bridge, or in other words increases the effective tunneling barrier, leading to a diminution of the electronic factor. This in turn suggests that conventional VAO perspectives (e.g., Rayleigh−Schrodinger perturbation theory) are subtly related to the Wentzel−Kramers−Brillouin (WKB) barrier perspective. The states that cause the greatest misrepresentation of the electronic factor are not intuitive from the VAO perspective; whereas in the VAO perspective the uppermost bridge states are deemed important in many particle-transfer ET models,[40,41] we find that exclusion of the lower bridge states causes problematical misrepresentation of the attractive nature of the bridge. Similarly, the transfer mechanism (particle, hole, mixed-mode) is related to the overall barrier height rather than the energy difference between the tunneling electron and the highest occupied molecular orbital (HOMO) or lowest unoccupied molecular orbital (LUMO), the latter being the standard VAO viewpoint. The relationship that we show between the WKB and VAO perspectives and how individual states affect the bridge role in ET has, to our knowledge, not previously been illustrated. In the next section, we briefly describe the quantum mechanics involved in ET processes such as superexchange, i.e., processes for which the rate expression is given by Fermi's Golden rule, and in a subsequent methods section we give technical details of how the present models are constructed. These sections are followed by a discussion of the results in which the main findings and their implications to biological ET are discussed in detail.

## II. Quantum Mechanics of Electron Transfer

Within the Born−Oppenheimer approximation electron transfer is described theoretically in the same fashion as any other chemical reaction. The nuclei move on one adiabatic potential energy surface that connects the donor and acceptor states and with the rate being determined by features of that potential energy surface. However, when the transition state between the donor and acceptor states is characterized by a weakly avoided crossing or when the donor and acceptor states are not on the same adiabatic surface, as in the inverted region of electron transfer, the Born−Oppenheimer approximation is not a good approximation and nonadiabatic processes must be considered to understand the electron-transfer process. Such a situation is typical in superexchange ET, and the preponderance of biological ET models are based on a nonadiabatic process. Usually the nonadiabatic processes are described using diabatic states. The diabatic states can be thought of as a set of electronic states of the system that can be written as linear combinations

of the complete set of adiabatic electronic states. There are various prescriptions for constructing these diabatic states that typically yield states with the following characteristics: (1) the diabatic states cross (i.e., are degenerate) at a geometry that is close to the geometry where the adiabatic states had an avoided crossing; (2) the diabatic states are localized with one state being a good description of the initial donor state and the other of the final acceptor state; (3) the diabatic states change slowly as a function of the position of the nuclei in the region of the crossing.[42]

In terms of the diabatic states, the electron-transfer rate expression for nonadiabatic electron transfer is given in first-order time-dependent perturbation theory by

$$k_{ET} = \frac{2\pi}{\hbar}|H_{DA}|^2 \rho_{FCWD} \tag{1}$$

where $H_{DA}$ is the electronic coupling matrix element between the diabatic donor and acceptor states and $\rho_{FCWD}$ is the Franck−Condon weighted density of vibronic acceptor states at the energy of the donor state. Often the diabatic states are not orthogonal. In that case the electronic coupling matrix element is given by[43]

$$H_{DA} = \frac{\langle \psi_D|H|\psi_A\rangle - E_{tun}S_{DA}}{1 - {S_{DA}}^2} \tag{2}$$

where $|\psi_D\rangle$ is the diabatic donor state, $|\psi_A\rangle$ is the diabatic acceptor state, $E_{tun} = \langle \psi_D|H|\psi_D\rangle = \langle \psi_A|H|\psi_A\rangle$ is the energy of the tunneling state, $S_{DA} = \langle \psi_D|\psi_A\rangle$, and $H$ is the total electronic Hamiltonian of the system. Note that this formula reduces to $H_{DA} = \langle \psi_D|H|\psi_A\rangle$ for the case of orthogonal diabatic states.

If the transition state occurs at a geometry where the donor and acceptor sites are equivalent, then there is a very simple choice for the diabatic states. The diabatic states can be constructed from the plus and minus linear combinations of the adiabatic states, where the adiabatic states are symmetric and antisymmetric with respect to a symmetry operation of the molecule that interchanges the equivalent donor and acceptor sites. If the energy of the adiabatic states are $E_a$ and $E_b$, the electronic coupling matrix element between the corresponding diabatic states is then

$$2H_{DA} = E_b - E_a = \Delta E_{split} \tag{3}$$

Equation 3 reveals that the splitting is indirectly related to the ET rate through the electronic factor $H_{DA}$.

There are a number of methods that have been used to compute the electronic factor for real systems. One class of computations uses self-consistent field (SCF) ab initio calculations where the diabatic states are obtained by solving for approximate localized SCF states either with or without a perturbation to localize the states. These calculations incorporate the full many-electron nature of the electronic state and have yielded coupling matrix elements that seem to be in good agreement with experimental data.[1,18,40] To study larger systems, investigators have employed more approximate calculations, usually invoking a single-particle approximation, i.e. assuming that the tunneling matrix element can be obtained by solving a Schrödinger equation that only contains the motion of a single electron moving under the influence of an interaction potential.[36,37,41,44] Once a single-particle Schrödinger equation is assumed, then it can be solved by direct diagonalization, using perturbation theory using expressions[40] similar to

$$H_{DA} = \sum_{B_{occ}} \frac{(\langle \psi_D|V_C|\psi_{B_{occ}}\rangle - E_{tun}S_{DB_{occ}})(\langle \psi_{B_{occ}}|V_C|\psi_A\rangle - E_{tun}S_{B_{occ}A})}{E_{tun} - E_{B_{occ}}} + \sum_{B_{unocc}} \frac{(\langle \psi_D|V_C|\psi_{B_{unocc}}\rangle - E_{tun}S_{DB_{unocc}})(\langle \psi_{B_{unocc}}|V_C|\psi_A\rangle - E_{tun}S_{B_{unocc}A})}{E_{tun} - E_{B_{unocc}}} \tag{4}$$

or a corrected version of perturbation theory as proposed by Katz and Stuchebrukhov.[45]

Newton[1] has described how it is possible to reduce what is at its most basic level a many-electron problem to a single-electron problem. He describes two possible cases. First, if the electron transfer is truly a single-particle process, with all of the electrons in the intervening medium (the bridge) not participating in the process, then the single electron can be thought of as moving in the mean field of the other electrons. This type of electron transfer is referred to as particle transfer. The other possibility is if the electrons of the bridge do participate. Then if one assumes that all of the electronic configurations that contribute to the electron-transfer process are just singly excited configurations relative to the donor initial electronic configuration, it is possible to show again that the many-electron Schrödinger equation can be transformed into a single-electron Schrödinger equation with an appropriate interaction potential. Such a process is referred to as hole transfer.

In this paper we will show that when hole transfer is significant, as determined by the probability fluxes, then a multiplicity of mixed-mode pathways will also be important, which cannot be described by single excitations relative to the donor state. Thus, the single-particle picture will not be valid when there is hole transfer. Another point we will graphically illustrate here is the difficulty in qualitatively interpreting a state-space solution of the electron-transfer problem. To answer questions concerning the impact that various parts of the bridge has on electron transfer, it is necessary to use a state-space expansion with localized nonorthogonal basis functions. As has been shown by Priyadarshy et al.,[46] it is essential to correctly treat the nonorthogonal nature of the basis set to obtain the correct electronic-coupling matrix element. The interpretation of wave functions constructed from such a basis set in terms of the expansion coefficients is ambiguous. In particular, if a tunneling state is seen to have a nonzero coefficient for a lower energy occupied bridge state, it is usually assumed that this is an indication that hole transfer is important in the electron-transfer process. The results presented here suggest that a better interpretation of such a wave function is that the tunneling state must be orthogonal to the occupied bridge state, and in a nonorthogonal basis set this necessarily requires a mixing of the bridge state with the tunneling state. Thus, the presence of a nonzero mixing coefficient with a bridge state does not imply the participation of that state in the tunneling process.

Although this brief review of quantum mechanical ET models has centered on the prevalent valence atomic orbital approach, the results from our configuration-space models have equally important implications for pathway models, which we discuss below. Another view on how to quantify the electronic factor is the barrier or WKB model. In the WKB model the tunneling matrix element is wholly dependent on the net potential barrier that the tunneling electron must traverse to reach the acceptor; considerations of the bridge electronic state energetics are irrelevant, and the sole utility of the bridge in promoting electron transfer lies in the effect the bridge nuclear potential

has in lowering the tunneling barrier. The standard rate expression for the WKB model[47] is

$$k_{ET}^{WKB} \propto \exp\left[-\frac{2}{\hbar}\int_{q_1^i}^{q_1^f}\{2[V(q_1) - E_{tun}]\}^{1/2}\,dq_1\right] = e^{-\Lambda R} \qquad (5)$$

where $V(q_1)$ describes how the barrier shape varies with the spatial coordinate, and we will refer to the WKB exponent defined here as $\Lambda$. The WKB picture of ET can be viewed in the context of the VAO approach in a manner that we demonstrate in the results section.

## III. Configurations-Space Model and Computational Methods

The central idea motivating our development of the present configuration-space model is that these models have significant advantages in visualizing the ET problem and hence in understanding explicitly the role of the bridge. Here, we will consider models in which each dimension represents an independent electron. To implement our configuration-space model computationally, we begin with a distributed Gaussian basis (DGB),[48] $\{|\phi_i\rangle\}$, and an electronic Hamiltonian given by

$$H = \sum_{i=1}^{N}\left(-\frac{1}{2}\frac{\partial^2}{\partial q_i^{\,2}} + V_{1D}(q_i)\right) \qquad (6)$$

where $N$ is the number of electrons in the system. In eq 6 each electron in the system is another dimension in the configuration-space model and is represented by the coordinate $q$ rather than by $x$, $y$, or $z$ to emphasize that the dimensionality of the model is related to the number of electrons in the system rather than to the spatial dimensions represented by Cartesian coordinates. The potential in the Hamiltonian is based on model Gaussians simulating the attractive potentials of the donor, acceptor, and bridge sites. The form of the 1-D potential is

$$V_{1D} = V_D(q_1) + V_A(q_1) + \sum_{\alpha=1}^{n} V_B(Q_\alpha, q_1) \qquad (7a)$$

where

$$V_D(q_1) = -c_{D/A}\exp\{-\beta_{D/A}(q_1 - R/2)^2\} \qquad (7b)$$

$$V_A(q_1) = -c_{D/A}\exp\{-\beta_{D/A}(q_1 + R/2)^2\} \qquad (7c)$$

$$V_B(Q_\alpha, q_1) = -c_B\exp\{-\beta_B(q_1 + Q_\alpha)^2\} \qquad (7d)$$

$$Q_\alpha = \left(\frac{\alpha}{n+1} - \frac{1}{2}\right)R \qquad (7e)$$

$n$ is the number of bridge sites, and $R$ is the distance between donor and acceptor.

To obtain the electronic factor for the model system, we construct the Hamiltonian matrix $H_{ij}$ over the DGB where the indices $i$ and $j$ indicate the DGB basis, symmetrically orthogonalize the basis set, transform $H_{ij}$ into $H_{ab}$ in the symmetrically orthogonal basis, and then diagonalize $H_{ab}$ to obtain the eigenvalues and eigenvectors. The energy difference between the quasi-degenerate donor acceptor states is $\Delta E_{split}$ and is related to the electronic factor by eq 3. These solutions to the problem in one spatial dimension and for one electron, designated $\{|\chi_a\rangle\}$, are very accurate solutions of our model problem. For the donor−bridge−acceptor potentials in our models, we find that approximately seven functions/bohr are required to converge the 1-D eigenvalues to $\sim 10^{-10}$ hartree, given an exponent of 15.00 for each Gaussian function in $\{|\varphi_i\rangle\}$. For the potential, using $c_D = c_A = -6.5$, $c_B = -11.0$, and $\beta_D = \beta_A = \beta_B = 5.0$ produces quasi-degenerate donor−acceptor values that are between and well separated from the two bridge eigenvalues, and for this reason we refer to this particular bridge as the "nonresonant bridge" below.

In addition to the exact solutions, we also considered solutions of our 1-D model problems in which we used a truncated basis set where each basis function was a solution to the 1-D problem with only one Gaussian potential well present (i.e., donor or acceptor or bridge only). These single-well solutions were then combined to solve the full multi-well D−B−A problem. This truncated basis set for our model problem is analogous to atomic centered basis sets used to solve the electronic structure in more realistic calculations of the ET electronic factor. Since we ultimately wanted to compare the VAO perspective to the WKB or barrier perspective, we used the formula

$$V^{eff} = \sum_{i,j}^{N_\phi}\sum_{a,b,c,d}^{N_{trunc}} |\phi_i\rangle\langle\phi_i|\chi_c\rangle(S^{-1})_{ca}\langle\chi_a|V|\chi_b\rangle(S^{-1})_{bd}\langle\chi_d|\phi_j\rangle\langle\phi_j| \qquad (8)$$

where $N_\phi$ is the number of DGB functions and $N_{trunc}$ is the number of states in the truncated basis, to see what approximate effective potential results from the truncated basis. Inserting this potential into the 1-D Hamiltonian will yield the same eigenvalues as the full potential when the Hamiltonian is solved in the same truncated basis set as is used to construct $V^{eff}$. This potential thus gives a way of visualizing how truncations of the basis set modify the underlying problem.

As electrons are added to the donor−bridge−acceptor system, this corresponds to adding dimensions to the configuration-space model. This enables us to add an electron−electron repulsion term, $V_{e-e}$, to the Hamiltonian. For $N$-dimensional solutions (where $N$ is the number of electrons and $N > 1$) including $V_{e-e}$, we perform a self-consistent field (SCF) calculation to find the $N$-dimensional wave functions for the ground-state configuration $||\chi_1\cdots\chi_N|\rangle^0$. This $N$-dimensional ground-state wave function contains an electron in the lower level of each bridge site plus one electron in the tunneling state. By removing the tunneling electron from the antisymmetrized, high-spin $||\chi_1\cdots\chi_N|\rangle^0$, we can construct a set of improved virtual orbitals (IVOs) for electronic states in the presence of an occupied bridge. Kurnikov et al.[40] have used the IVO method in models of intramolecular ET in a bimetallic system and have found that this methodology provides a better description of excited states of the system. Construction of the IVOs results in a new set of one-electron states, $\{|\chi_a^{IVO}\rangle\}$ that we use in configuration state functions (CSFs) composed of antisymmetrized direct products of IVOs, or $\{||\chi_1^{IVO}\cdots\chi_N^{IVO}|\rangle\}$. A few of these one-electron IVO states are bound orbitals, but the majority of them are continuum functions that, when included in the set of CSFs, contribute little to the CI results but increase the cost of the computation greatly. Thus, we choose a subset of these states, indicated by the index $S$, and compute CI eigenvalues of the full $N$-dimensional Hamiltonian using the linear variational method and $\{||\chi_1^{IVO}\cdots\chi_N^{IVO}|\rangle_s\}$.

To consider the effect of $V_{e-e}$, we constructed a delocalized Coulomb potential from a linear combination of three Gaussian functions,

$$V_{e-e}(q_1, q_2) = \sum_n c_n\, e^{-\beta_n(q_1 - q_2)^2} \qquad (9)$$

and add this to the Hamiltonian. We then solve the correspond-

**TABLE 1: Expansions of the $J$ and $\tilde{K}$ Integrals Used to Construct $V_{2D}$ As Given in Eq 10[a]**

| | bridge description | | | |
|---|---|---|---|---|
| | nonresonant | Int. 1 | Int. 2 | nearer-resonant |
| $J_1$, $c/\beta$ | 4.991/6.165 | 4.671/5.860 | 4.420/5.639 | 4.003/5.483 |
| $J_2$, $c/\beta$ | 2.987/1.951 | 3.053/1.897 | 3.103/1.852 | 3.248/1.846 |
| $J_3$, $c/\beta$ | 0.755/0.0902 | 0.755/0.0902 | 0.756/0.0901 | 0.770/0.0905 |
| $\tilde{K}_1$, $c/\beta$ | 3.644/8.412 | 3.418/7.989 | 3.256/7.676 | 4.450/6.577 |
| $\tilde{K}_2$, $c/\beta$ | 4.096/4.842 | 3.951/4.478 | 3.870/4.189 | 2.786/2.979 |
| $\tilde{K}_3$, $c/\beta$ | −0.370/2.335 | 0.430/2.129 | 0.433/1.912 | 0.0155/0.147 |

[a] The Gaussians used to expand the $J$ and $\tilde{K}$ operator are centered at the center of the bridge well.

ing Schrödinger equation as described in the paragraph above. The coefficients and exponents of the three Gaussians used to construct the approximate $1/r$ Coulomb potential are $c_1 = 19.218$, $c_2 = 2.660$, and $c_3 = 0.754$ and $\beta_1 = 58.501$, $\beta_2 = 2.598$, and $\beta_3 = 0.0910$, respectively. The results from calculations including $V_{e-e}$ are not directly comparable to results from the same calculation in the absence of $V_{e-e}$ because the inclusion of repulsion alters the bridge eigenstate levels. To obtain a bridge electronic structure with eigenstates close to those of the bridge in the absence of repulsion, we subtract terms of the form $J_B - \tilde{K}_B$ at the same time as we add in the $V_{e-e}$ repulsion. The term $J_B$ is the Coulomb integral, which gives the interaction of the tunneling electron with an electron in the state used to construct the IVOs (i.e., a state wherein bridge sites have an electron in the lower energy state), and $\tilde{K}_B$ is a local approximation to the exchange interaction with an electron in the same state. Thus, our 2-D potential that includes electron−electron repulsion has the form

$$V_{2D} = V(q_1,q_2) = V_{1D}(q_1) + V_{1D}(q_2) + V_{e-e}(q_1,q_2) - (J_B(q_1) - \tilde{K}_B(q_1)) - (J_B(q_2) - \tilde{K}_B(q_2)) \quad (10)$$

The exchange integrals are approximated by the diagonal elements of their respective matrices in the DGB. The $J_B$ and $\tilde{K}_B$ approximations are also expressed as the linear combination of three Gaussian functions. Table 1 gives a description of the coefficients and exponents used to approximate $J_B$ and $\tilde{K}_B$ for four different 1-D bridge potentials used in the two-electron models discussed in this work. In $V_{1D}$, the same value of $\beta$ is used for all bridges (5.0), and intermediate bridge 1 (Int. 1), intermediate bridge 2 (Int. 2), and the nearer-resonant bridge have $c_B = 9.5$, $c_B = 8.5$, and $c_B = 7.5$, respectively. After obtaining expressions for $V_{e-e}$, $J_B$, and $\tilde{K}_B$, we may perform a calculation with $V_{e-e}$ that will be comparable to the calculation without by subtracting the approximate $J_B - \tilde{K}_B$ from the 1-D potential at the outset of the calculation.

To fully realize the advantages of the configuration-space model, we need to calculate tunneling fluxes. To do this, we first use the delocalized symmetric and antisymmetric CI solutions ($|\Psi^+\rangle$ and $|\Psi^-\rangle$) to construct localized donor and acceptor CI wave functions

$$|\Psi_D\rangle = \frac{|\Psi^+\rangle + |\Psi^-\rangle}{\sqrt{2}} \quad \text{and} \quad |\Psi_A\rangle = \frac{|\Psi^+\rangle - |\Psi^-\rangle}{\sqrt{2}} \quad (11)$$

Using $|\Psi_D\rangle$ and $|\Psi_A\rangle$, we calculate the donor-to-acceptor tunneling flux from the relation

$$j_i(q_1 \cdots q_N,t) = \left(\Psi^- \frac{d\Psi^+}{dq_i} - \Psi^+ \frac{d\Psi^-}{dq_i}\right) \sin(t\Delta E_{split}) \quad (12)$$

where $t$ is time and the wave functions are real.

**SCHEME 1: Potential Structure for Donor−Bridge−Acceptor System with the "Nonresonant" Bridge**

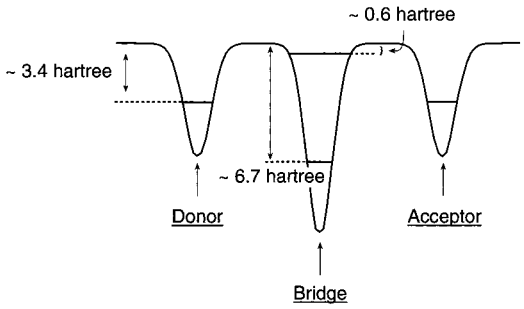


## IV. Results and Discussion

**A. Effect of Excluding Selected Bridge States from the Model.** We discussed above how in models of large biological systems some states may be excluded from the model. We begin by using the simple 1-D model to see what effect this type of approximation has on the electronic factor by comparing approximate results to exact results for the same system. We begin by considering a simple donor−bridge−acceptor (D−B−A) system described above where the bridge is nonresonant; i.e., the bridge bound states are well separated from those of the donor and acceptor. In the present case, because we are considering a model system, what is meant by the terms donor, bridge, and acceptor is somewhat abstract. We want to address issues in how large-scale models of biological ET are constructed, and many large-scale biological models describe systems in which two metal centers with near-degenerate d levels are separated by a nonmetal protein matrix that has bound states above and below the d levels but no bound states that are energetically near the d levels.[37] Examples of similar but smaller ET systems are also common and include the system studied by Kurnikov et al. in which an Ir donor atom transfers an electron to an Ir acceptor atom through a covalently bonded pyrazolate bridge, and a separate work of ours in which we look at the electron transfer from an iron donor to an iron acceptor through a nonbonded water bridge. Thus, the models constructed here utilize quasi-degenerate donor and acceptor states that are energetically well separated from the bridge bound states. Scheme 1 depicts the potential for the D−B−A system with a nonresonant bridge in which the diabatic donor and acceptor bound states have a binding energy of −3.4 hartree and the upper and lower bound states for the isolated bridge are at −0.6 and −6.7 hartree, respectively.

In Figure 1 the electronic factor $\Delta E_{split}$, which is directly related to the electronic factor portion of the ET rate, is plotted as a function of the distance between the donor and acceptor for both exact and approximate solutions of the DBA system in Scheme 1. In this calculation, we first obtain the exact solution and then compare this to solutions that include only selected bound states in the model per the description of the truncated basis in section III. The "approximate" solution using all four bound states is the same as the exact solution in Figure 1 to the scale resolvable on the graph, and both of these are given by the solid line. If we selectively exclude bound states from the calculation, we begin to see some interesting effects. In Figure 1 we see that the splittings found by excluding the higher energy bridge bound state compare reasonably well to the full solution, but if the lower energy bridge state is excluded, the accuracy of the splitting compared to the exact solution is significantly compromised and is nearly the same as that of a donor−acceptor system with no promoting bridge whatsoever, i.e., the bottom-most line in Figure 1. Also in Figure 1 we see that even if no

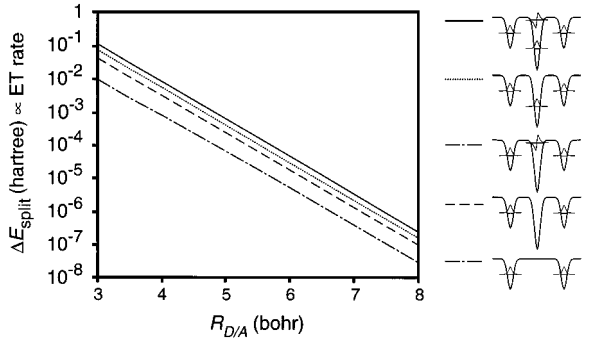


**Figure 1.** $\Delta E_{split}$ as a function of donor−acceptor separation, $R_{D/A}$, and the effect of excluding selected bridge states. Including both bridge states (solid line) is the same as the exact solution to within the scale of the graph, but, by comparison, excluding either of the bridge states results in errors in the electronic factor. $\Delta E_{split}$ obtained using only the upper bridge state and $\Delta E_{split}$ with no bridge give the same results to within the scale of the graph and are represented by a single line.

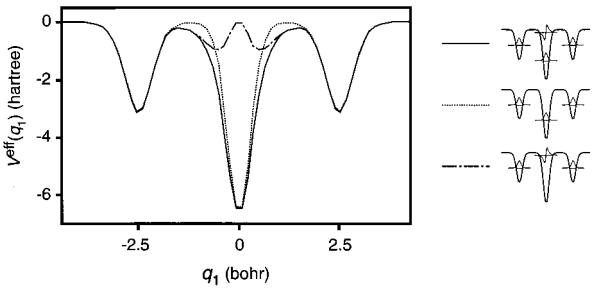


**Figure 2.** Diagonal elements of $V^{eff}$, the effective bridge potential, as a function of the bridge states used in the simplifying approximation. $V^{eff}$ is defined in eq 8.

bridge states are explicitly included and we use only the donor and acceptor states, the splitting is enhanced by the presence of an attractive potential between the donor and acceptor centers.

To place the results in Figure 1 in the context of large ET models for protein systems where a limited state-space is chosen in order to make such models tractable, we consider the example of the work by Kuki and Wolnyes.[31] These authors used repulsive pseudopotentials to produce bridge sites each of which had only one bridge bound state that was higher in energy than the bound donor−acceptor. The use of the pseudopotential not only reduced the size of the calculation by reducing the number of bridge states that needed to be included, but it was also necessary to successfully implement the pathway model used by the authors. Pseudopotentials often fail to capture the essence of the very attractive nuclear potential, and we believe their use should be approached with caution in these types of problems. Using the analogous practice in Figure 1, i.e., including only the most loosely bound bridge state, produced a splitting that was the same as that for ET without the promoting effect of the bridge (lowest line, Figure 1). We conjecture that this drastic underestimation of the electronic factor arises in part because of the effective exclusion of important parts of the bridge attractive potential when the strongly bound state is excluded, much like the repulsive core pseudopotential of Kuki and Wolynes does not support any bound states below the donor−acceptor energy level.

To find out more about the effect of the approximations discussed in Figure 1, we used eq 8 to calculate the effective potential, $V^{eff}$, for each approximate solution and plot the diagonal elements in $V^{eff}$ as a function of $q_1$ in Figure 2. The effective potential gives a way of visualizing how excluding selected states from the model modifies the underlying ET

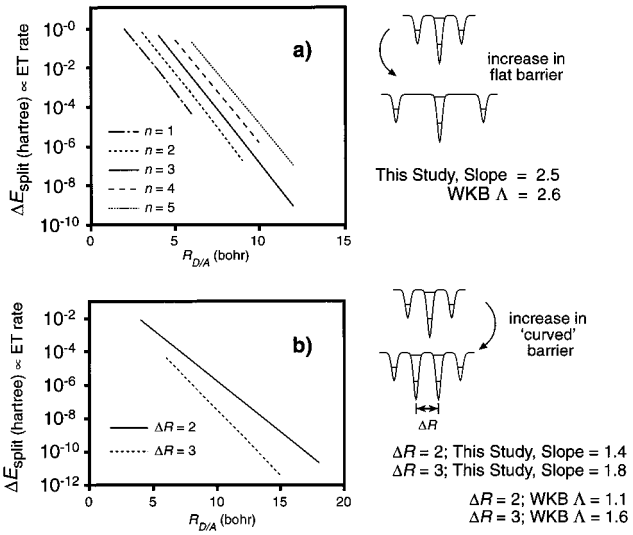


**Figure 3.** Configuration-space model results showing the effect on $\Delta E_{split}$ of increasing (a) the flat and (b) the curved barrier in the space between donor and acceptor. To the right of each graph the slope of $\ln(\Delta E_{split})$ as a function of the distance between the donor and acceptor is compared to the slope Λ predicted by WKB theory using eq 5. $\Delta R$ is the distance between centers of neighboring wells.

process. A look at Figure 2 immediately reveals the reason some approximations are better than others. The approximate solution using all four bound states in the model has an effective potential that is, to the scale of the graph, the same as the exact potential. When the higher energy bridge state out of the calculation is left out, the effective potential exhibits a slightly higher barrier around the bridge, and this lowers the splittings for this approximation in Figure 1, a result that would lead to inaccuracies in the calculated ET rate. Excluding the lower energy state from the model results in an effective potential that fails to represent the attractive nature of the bridge, has a much higher barrier to tunneling, and produces an electronic factor that is much too low. Although $V^{eff}$ is only an approximate localized potential, Figure 2 gives an excellent qualitative picture of how excluding selected states from the model (or analogously, use of a repulsive core pseudopotential) may fail to represent the critical aspect of the deeply attractive bridge potential that promotes long-range ET.

**B. Comparison of Model Results to WKB Predictions.** The idea that excluding selected states from the ET model might deleteriously affect the calculated ET rate because it implicitly excludes some of the bridge attractive potential has direct implications for barrier, or WKB, models of tunneling. Figure 3 shows how the exact results from this model compare to WKB predictions using eq 5. We find that the barrier model predictions are in excellent agreement with our model results, even though our system may not strictly adhere to the qualifying assumptions pertinent to the WKB model[49] (i.e., that the potential varies slowly and that the two turning points be well separated). This agreement between our model results and WKB theory predictions is excellent for variations in the flat barrier between donor and acceptor, when only the distance between donor and acceptor is varied (Figure 3a). The agreement is still good but less quantitative for variations in the curved barrier between donor and acceptor (Figure 3b), in other words when new bridges are added between the donor and acceptor. This is probably because in this latter case the potential is not varying slowly. Of course, the simple barrier model is one of the oldest and most thoroughly considered ET models, and as such, it is generally agreed to be inadequate of itself as a predictive basis

**SCHEME 2: Bridge-Dependent Mechanism of Superexchange**

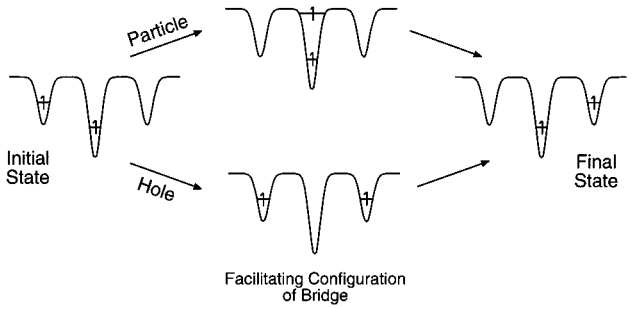


for modeling bridge-mediated ET in proteins; other important factors that a model must incorporate are symmetry and the interference between through-bond and through-space transfer paths.[25,42,50−52] The model system that we are treating here considers through-bond interactions, and we treat the other topics in a separate work.[53] However, for the through-bond interactions that we are treating here, the attractive potential of the bridge is the major rate-determining consideration. The other factors we mention (e.g., interference) are typically *rate-vitiating* considerations that are not inimical to the basic idea that the bridge attractive potential is the major promoting factor in biological ET by superexchange. We expect that for some complex protein systems the donor−acceptor separation is sufficiently great that there is no competitive or interfering through-space path and that the electronic factor contribution to the ET rate is as simply predicted by the barrier structure as the WKB model would suggest.

**C. Two-Electron Models and ET Transfer Pathways: Particle vs Hole?** So far, we have considered results from a system in which the only particle influencing the tunneling rate is the tunneling electron. By increasing the number of interacting electrons in the system, we can utilize our configuration-space model to look at the effects of electron−electron repulsion, $V_{e-e}$, and competitive transfer pathways in configuration-space. Additionally, we can look at the issue of particle vs hole transfer. To first look at the particle vs hole transfer issue, we begin with the simple 2-D system depicted in Scheme 2 in the absence of electron−electron repulsion ($V_{e-e} = 0$). Scheme 2 illustrates the difference between these two transfer mechanisms; both particle and hole transfer have the same initial and final states, but the facilitating role of the bridge is very different in each case. It is important to note here our use of the phrase "facilitating configuration". The D−B−A configurations such as those in Scheme 2 lend the impression of chemical intermediates in which a transferring electron or hole may be localized on the bridge; however, these schemes are meant to aid the reader's understanding of how the model works, not to represent how superexchange ET occurs. The bridge configurations are useful to identify the manner in which the bridge mediates the ET transfer process, but the process itself is not affiliated with sequential electron or hole hopping and should instead be viewed as an electron probability leak that flows from the donor into the acceptor via the bridge and as a result of the facilitating configurations that the bridge enables.

In Scheme 2 the bridge configuration that facilitates particle transfer results when an electron is added to the higher energy bridge site, or the site corresponding to the LUMO in molecular systems. In contrast, the bridge configuration that facilitates hole transfer results when an electron is removed from the lower

**SCHEME 3: 2-D Configuration-Space Model**

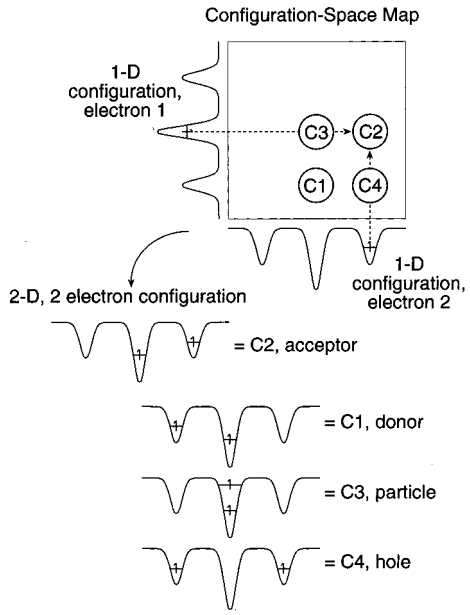


energy bridge site, or the site corresponding to the HOMO in molecular systems. Because tunneling matrix element expressions based on second-order perturbation theory contain terms such as $(E_{tun} - E_B)^{-1}$, an electronic energy gap, the importance of particle transfer is usually interpreted in terms of the energy gap between the protein bridge's LUMO and $E_{tun}$ (i.e., $(E_{tun} - E_{B_{unocc.}})^{-1}$; see eq 4). Likewise, the importance of hole transfer is usually interpreted in terms of the energy gap between the protein bridge's HOMO and $E_{tun}$ (i.e., $(E_{tun} - E_{B_{occ.}})^{-1}$; see eq 4). The usual conclusion is that particle transfer dominates over hole transfer when the tunneling energy, $E_{tun}$, is closer to the protein bridge LUMO than it is to the HOMO, and this type of analysis may even extend to other formalisms for ET models.[26,29,40,41] We propose that this perspective is misleading and will examine the question more fully in our model.

Scheme 3 illustrates how the configuration-space model can be visualized for a 2-D model system. In this model each dimension represents an independent electron. Hence, when electron 1 is in the lower level of the bridge well and electron 2 is in the acceptor well, the wave function is localized in the region C2 of the 2-D space as indicated in Scheme 3. The value of this configuration-space approach will be apparent when we look at tunneling fluxes because this model enables us to trace the configuration pathways through which electron transfer occurs. In both Schemes 2 and 3, only two electrons are shown in the donor−bridge−acceptor complex. In practice there are many more electrons in the system, but core and inner valence electrons do not typically enter into thermal or photoinduced ETs.

Parts a and b of Figure 4 show the donor → acceptor flux for a bridge structure such that $E_{part.} - E_{D/A} \approx E_{D/A} - E_{hole}$, and the configuration-space potential, respectively. The quantities $E_{part.}$ and $E_{hole}$ are the energies of the states representing particle and hole-transfer facilitators, respectively (see Scheme 2), and $E_{D/A}$ is the energy of the initial/final state, which, as previously mentioned, has the same configuration regardless of the transfer mechanism. The multidimensional configuration-space model potential is the sum of the independent 1-D potentials from eq 7a. In this case the energy of the tunneling electron is approximately halfway between and well separated from the energies of the bridge HOMO and LUMO, i.e. the

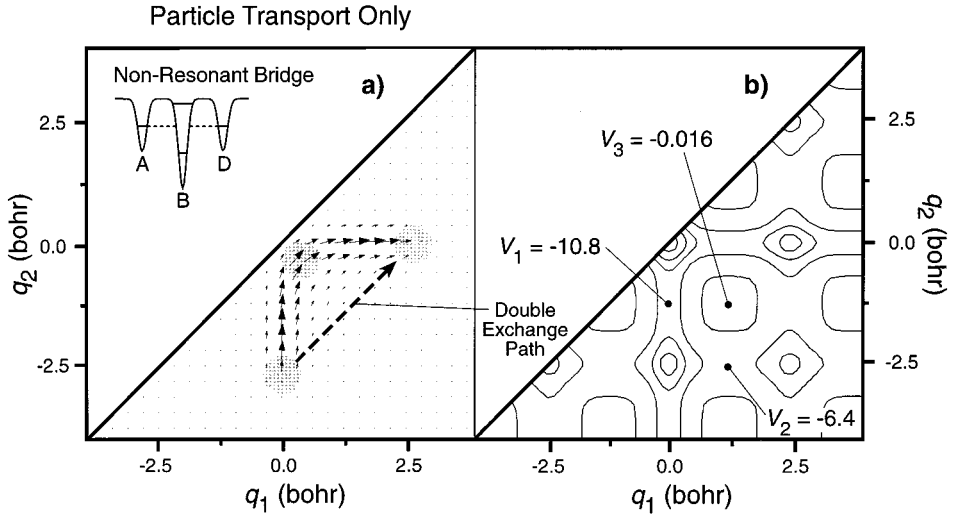


**Figure 4.** 2-D configuration-space ET for a nonresonant bridge. (a) Flux, represented by arrows, passes from the donor to the acceptor through a particle-transfer configuration. Gray circles correspond to C1, C2, and C3 in Scheme 3. (b) Configuration-space potential contours corresponding to the nonresonant D−B−A structure. The 1-D potential in Figure 1 with a donor−acceptor separation, $R_{D/A}$, of 5.0 bohr is used to construct the 2-D potential; energy contours are at −1.0, −6.8, −11.0, −14.0, and −17.0 hartree. The tunneling state energy is −10.09 hartree, and $V_1$ and $V_2$ are saddle points for the particle and hole pathways. $V_3$ is the maximum in the potential along the double exchange pathway shown by the dashed line in (a). $\Delta E_{split}$ is in Table 3.

**TABLE 2: Eigenvalues of 2-D CI Matrix and Energy Gaps between the Donor−Acceptor and Bridge States**

| | bridge description | | | |
|---|---|---|---|---|
| | nonresonant | Int. 1 | Int. 2 | near-resonant |
| | Eigenvalues,[a] hartree | | | |
| without $V_{e-e}$ | | | | |
| $E_{C1/C2}$ | −10.09 | −8.96 | −8.22 | −7.50 |
| $E_{C2}$ | −7.29 | −5.83 | −4.93 | −4.12 |
| $E_{C3}$ | −6.80 | −6.80 | −6.80 | −6.80 |
| with $V_{e-e}$ | | | | |
| $E_{C1/C2}$ | −11.20 | −10.09 | −9.36 | −8.65 |
| $E_{C2}$ | −8.18 | −6.83 | −6.00 | −5.24 |
| $E_{C3}$ | −7.58 | −7.58 | −7.58 | −7.58 |
| | Energy Gaps,[b] hartree | | | |
| without $V_{e-e}$ | | | | |
| $E_{part} - E_{D/A}$ | 2.8 | 3.1 | 3.3 | 3.4 |
| $E_{D/A} - E_{hole}$ | 3.3 | 2.2 | 1.4 | 0.7 |
| with $V_{e-e}$ | | | | |
| $E_{part} - E_{D/A}$ | 3.0 | 3.3 | 3.4 | 3.4 |
| $E_{D/A} - E_{hole}$ | 3.6 | 2.5 | 1.8 | 1.1 |

[a] See Scheme 3 for state configurations. Eigenvalues were obtained by diagonalizing the 4 × 4 CI matrix that was generated using IVO orbitals, as discussed in the text. Note that C1 and C2 are nearly degenerate states, one of which is symmetric and one of which is antisymmetric, and the splittings between these two states are given in Table 3. [b] $E_{part} - E_{D/A} = E_{C3} - E_{C1/C2}$ and $E_{D/A} - E_{hole} = E_{C4} - E_{C1/C2}$. Note that because of the weak interaction in these model systems, the differences are small between the final eigenvalues and the value of the diagonal elements in the original basis set.

nonresonant bridge. The 2-D CI eigenvalues and the energy gaps $E_{part.} - E_{D/A}$ and $E_{hole} - E_{D/A}$ are in Table 2. Essentially all of the tunneling flux in Figure 4a is passing through the particle-transfer configuration (region C3 in Scheme 3), and in Figure 4b it is apparent that this bridge configuration represents a strongly attractive intermediate with a low-energy transition state designated $V_1$ in the figure. Note that the 1-D model potential on which the 2-D model is based has a tunneling barrier. In Figure 4b, there is no barrier to tunneling along each 1-D leg of the particle-transfer path (the energy of the tunneling state is −10.09 hartree. and the particle-transfer saddle point energy is −10.80 hartree). However, because the lowest energy bound state in a 11.0 hartree deep 1-D potential is −6.7 hartree (vida supra), we conclude that by inclusion of the transverse modes adiabatically there would be an effective one-dimensional tunneling barrier.

We contrast the case of the nonresonant bridge with what we shall designate the nearer-resonant bridge in which one of the bridge levels has an energy closer to that of the donor−acceptor increasing the strength of the coupling between the bridge and the donor−acceptor. The energy gap between the donor−acceptor state and the nearest bridge level for the nearer-resonant bridge from Table 2 is 0.7 hartree or 19.0 eV. This energy gap is substantial and is significantly greater than typical gaps for molecular systems,[37] but the energies for bound states in molecular systems are not directly comparable to the model system that we treat here, and we do not require this direct comparability, since the current model is used to examine ET dynamics rather than for predictive purposes. The ET flux and configuration-space potential for the nearer-resonant bridge are plotted in Figure 5. The manner in which we construct the nearer-resonant bridge is apparent from the configuration-space potential in Figure 5b; the bridge attractive potential is decreased until the lower bridge eigenstate comes closer to the donor and acceptor levels. This has the net effect of making the effective hole-transfer barrier comparable to the particle-transfer barrier, and as a result, a little more than half of the total ET flux passes through the hole-transfer configuration. Note that even for the nearer-resonant bridge, hole transfer is an important transfer mechanism, but it is not the only important transfer process as particle transfer was in the case of the nonresonant bridge.

Scheme 4 allows us to more easily view results from the two-electron models in the context of the WKB perspective on tunneling. In the top portion of Scheme 4 we see how the tunneling barrier for particle transfer is lower than that for hole transfer when the nonresonant bridge is between the donor and the acceptor, and we previously saw how ET with the nonresonant bridge is dominated by a single transfer mechanism, that being particle transfer. In the bottom panel of Scheme 4 we see a diagram of what the barrier to particle and hole transfer is for the nearer-resonant bridge. In the case of the nearer-resonant bridge the barrier for the former is very similar to that of the latter, and hence, both particle and hole transfers are important

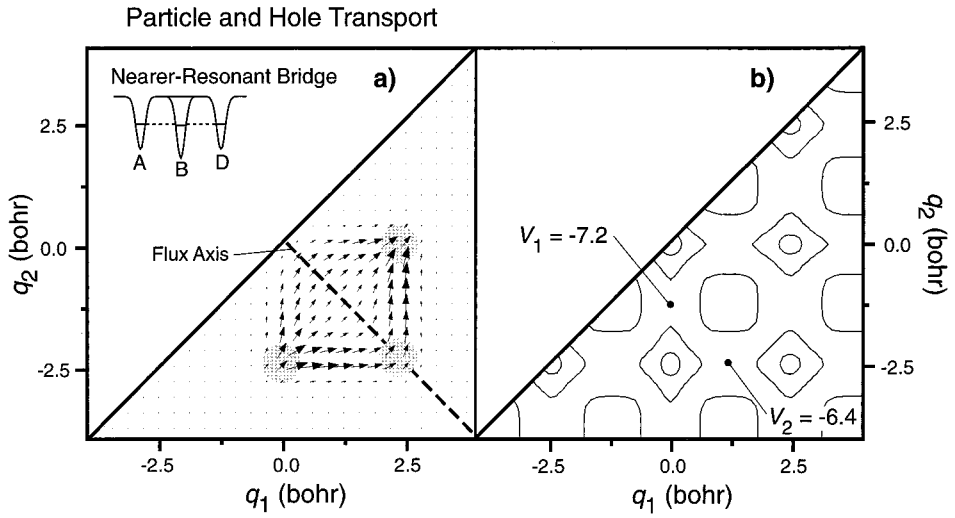


**Figure 5.** 2-D configuration-space ET for a nearer-resonant bridge. (a) Flux, represented by arrows, passes from the donor to the acceptor through both particle- and hole-transfer configurations. Gray circles correspond to C1, C2, and C4 in Scheme 3 and emphasize the hole-transfer path, and the dashed line indicates the flux axis used to analyze flux pathways. (b) Configuration-space potential contours corresponding to the nearer-resonant D−B−A structure. The 2-D potential is constructed from the 1-D potential for the nearer-resonant bridge discussed in the text with a donor−acceptor separation, $R_{D/A}$, of 5.0 bohr; energy contours are at −1.0, −6.8, and −11.0 hartree. The tunneling-state energy is −7.50 hartree, and $V_1$ and $V_2$ are saddle points for the particle and hole pathways.

**SCHEME 4: Diagram of Particle and Hole Tunneling Barriers for Nonresonant and Nearer-Resonant Bridges**

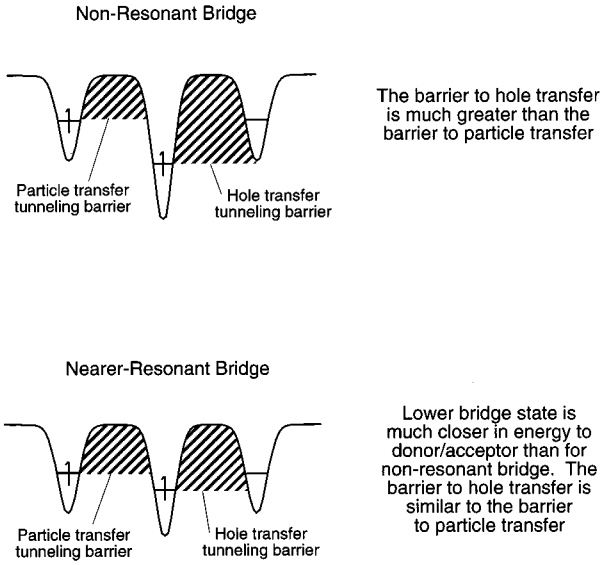


in ET with the nearer-resonant bridge. From the perspective of Scheme 4 it is apparent why hole transfer will never be the single dominant transfer mechanism in superexchange; there is no bridge configuration for which the barrier-to-hole transfer is lower than the barrier-to-particle transfer as long as the occupied bridge levels are lower in energy than the donor−acceptor levels in which the transfer is occurring. We noted above how diagrammatic representations such as Schemes 1−3 evoke a state-space image of superexchange that may be misleading inasmuch as it suggests that the transferring electron (or hole) may be localized on the bridge during the ET when actually superexchange ET occurs via a delocalized intermediate. Nonetheless, Schemes 1−3 are very useful for visualizing various issues related to superexchange ET, and Scheme 4 provides a unifying glimpse at why (though schemes such as Schemes 1−3 are useful in conceptualizing the transfer mechanism) the contour plots in Figures 4b and 5b are the more realistic way to view the problem.

**D. Two-Electron Models: The Effect of Electron−Electron Repulsion.** We now want to examine how electron−electron repulsion affects both the magnitude of the electronic factor and the transfer mechanism. We noted in the methods section that results from model calculations including $V_{e-e}$ are not directly comparable to results from the same calculation in the absence of $V_{e-e}$ because the inclusion of repulsion alters the bound-state energy levels in the bridge, and we outlined an approximation technique, using eq 10, by which we can construct bridges that, in the presence of $V_{e-e}$, are comparable to a bridge in a system without $V_{e-e}$. The resulting bridge eigenvalues, given for the four different bridges in Table 2, are much closer to those of the same bridges in the absence of repulsion than they would be without using this approximation. The quantities $E_{part.} - E_{D/A}$ and $E_{hole} - E_{D/A}$, also in Table 2, are the energy differences, respectively, between the particle and hole configurations in Scheme 3 and the initial/final configuration. A comparison of the 2-D model with and without $V_{e-e}$ shows that these energy differences are very similar. In parts a and b of Figure 6 we give the flux and potential for the 2-D nonresonant bridge model with a potential incorporating $V_{e-e}$. Although the repulsion is clearly evident in the potential, the flux still passes predominantly through the particle-transfer configuration.

In the flux diagrams of Figures 4a, 5a, and 6a all of the net ET flux must pass through the 2-D flux axis depicted in Figure 5a. We utilize this flux axis in Figure 7 to plot the total flux magnitude at each point across the axis for ET transfer across the nonresonant well, the nearer-resonant well, and two intermediate cases wherein the more strongly bound bridge eigenstate is gradually moving closer to the donor and acceptor. In Figure 7a there is no electron−electron repulsion and the flux magnitudes for the near-resonant and nonresonant bridges correspond to the fluxes from Figures 4a and 5a. In Figure 7b the flux magnitudes result from calculations including $V_{e-e}$ using bridges comparable to those used in the absence of repulsion, and the nonresonant flux magnitude corresponds to that of Figure 6a. The logical expectation is that the addition of electron−electron repulsion to the system should increase the relative proportion of hole transfer, since the tunneling electron

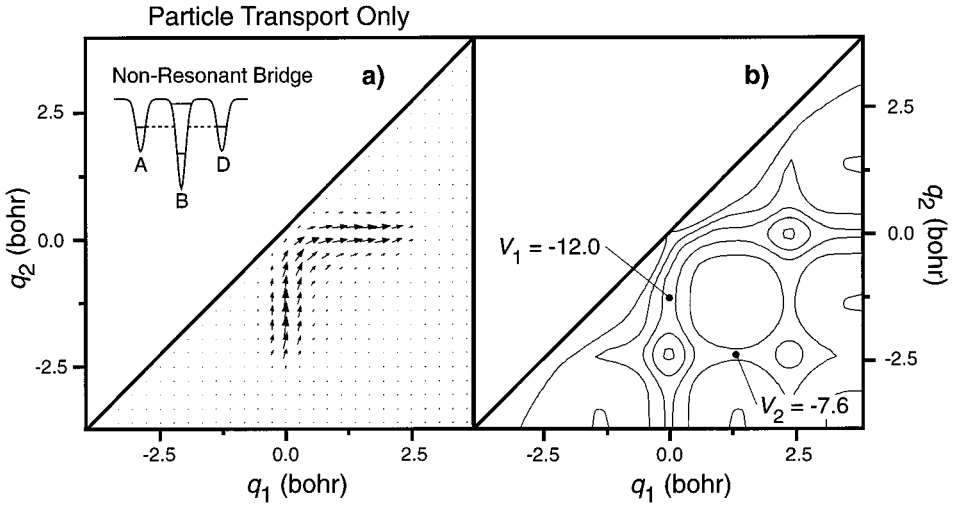


**Figure 6.** 2-D configuration-space ET for a nonresonant bridge where effects of electron−electron repulsion are included. (a) Flux, represented by arrows, passes mostly through a particle-transfer configuration. (b) Configuration-space potential contours corresponding to the nonresonant D−B−A structure. The 2-D potential (eq 10) with a donor−acceptor separation of $R_{D/A} = 5.0$ bohr is constructed to mimic the bridge used in Figure 4 by a technique described in the text using eq 10. Energy contours are at −1.0, −6.8, and −11.0 hartree. The tunneling-state energy is −7.50 hartree, and $V_1$ and $V_2$ are saddle points for the particle and hole pathways.

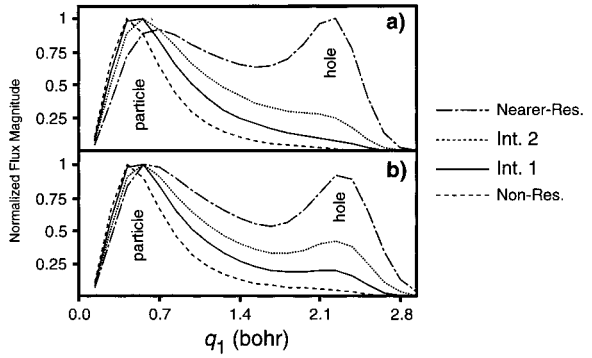


**Figure 7.** Relative proportion of particle and hole transfers as a function of the bridge structure. Flux magnitudes are taken along flux axis defined by $q_1 = -q_2$ and indicated in Figure 5. (a) No electron−electron repulsion. (b) With electron−electron repulsion.

**TABLE 3: Comparison of ET Rate for 2-D D−B−A Systems Solved with and without Electron−Electron Repulsion**

| | $\Delta E_{split}$, $10^{-4}$ hartree | | |
|---|---|---|---|
| bridge | without $V_{e-e}$ | with $V_{e-e}$ | % difference |
| nonresonant | 6.33 | 6.79 | +7 |
| Int. 1 | 6.74 | 7.56 | +11 |
| Int. 2 | 8.19 | 9.12 | +11 |
| near-resonant | 13.40 | 13.24 | −1 |

is now repulsive and could slightly increase the probability of the electron in the lower bridge state transferring to the acceptor (producing a hole-transfer configuration). What we observe in Figure 7b is a slight increase in hole relative to particle transfer, compared to Figure 7a, which is primarily noticeable as the bridge is nearer resonance. Table 3 compares the electronic factor contribution to the ET rate with and without $V_{e-e}$ for the nonresonant, near-resonant, and two intermediate bridges considered in Figure 7. In general, the electronic factor contribution to the ET rate for bridges with $V_{e-e}$ is comparable to, but higher than, the ET rate for corresponding bridges in the absence of $V_{e-e}$. We expect this not from energy gaps, which all favor increased ET for the D−B−A in the absence of $V_{e-e}$ (Table 2), but rather from the lower eigenvalues resulting for the states with $V_{e-e}$. The eigenvalues from calculations incorporating $V_{e-e}$ are lower because of changes to the bridge potential structure, while the donor and acceptor remain essentially the same as in the calculation without $V_{e-e}$. This means that there is less barrier to ET (or a more attractive bridge potential) in the models with $V_{e-e}$. By looking at the normalized rather than absolute flux magnitudes, we can assign the slight but discernible quantitative enhancement of hole over particle transfer that appears in Figure 7b to the effects of $V_{e-e}$.

There is another possible transfer pathway that we have neglected to mention so far and that is double exchange.[1] In the case of the 2-D system, double exchange amounts to the bridge electron transferring to the acceptor while the donor electron is simultaneously transferring to the bridge. In Figures 4a and 5a this pathway corresponds to flux passing directly along a straight line from the donor configuration to the acceptor configuration (see bold dashed line in Figure 4a). Double exchange is a transfer mechanism that should be enhanced by electron−electron repulsion for the same reasons we cite for hole transfer, a reason that is perhaps even more germane to double exchange. In Figure 7a the shape of the nonresonant well flux magnitude along the flux axis has a slowly dying tail along the part of the flux axis corresponding to double exchange ($q_1 \approx 1.4$ bohr on the flux axis) indicating that some small flux contribution arises from double exchange, even without electron−electron repulsion. For the realistic Coulomb electron−electron repulsion in Figure 7b this contribution is not significantly enhanced. We have found however that when a very high and physically unrealistic repulsion is chosen, a third discernible double exchange flux magnitude centroid arises between the hole- and particle-transfer centroids. Note that double exchange occurs along the configuration-space path with the highest tunneling barrier ($V_3$ in Figure 4b), and in regard to Scheme 4, we see that double exchange is not an important transfer path because the tunneling barrier for double exchange is the sum of both hole- and particle-transfer barriers.

**E. Three-Electron Models and ET Transfer Pathways: Evolution of Path Multiplicity.** From the 2-D configuration-space system, we conclude that electron−electron repulsion is not of great importance in affecting the ET mechanism. To further investigate the effect of multielectron effects on the transfer mechanism, we add another bridge to our system and look at the configuration-space model results for the moiety D−B−B−A, where the two bridge potentials are identical, each

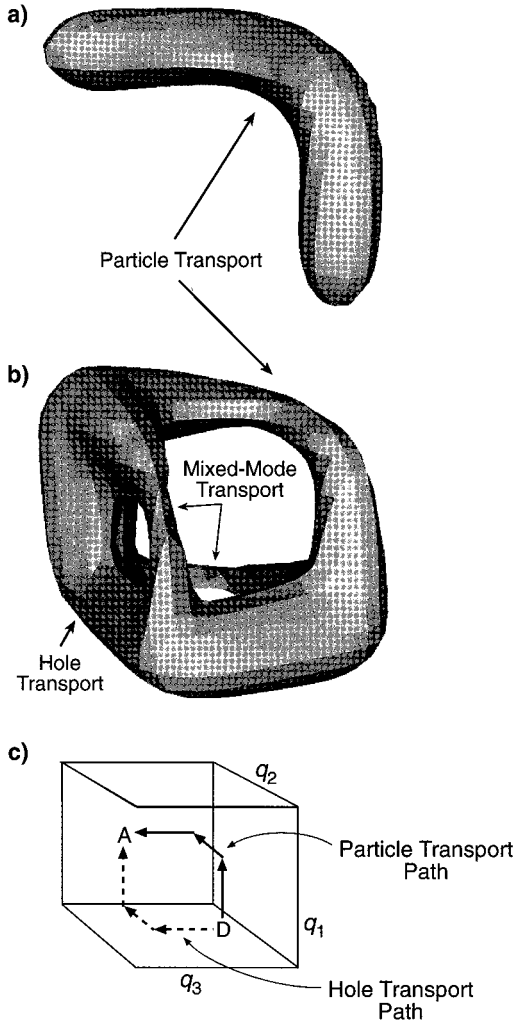


**Figure 8.** 3-D configuration-space model results. The 3-D potential is constructed from the appropriate 1-D potentials as described in the text, and the donor−acceptor separation is $R_{D/A} = 7.5$ bohr. (a) 3-D flux for a nonresonant bridge and 1-D parameters describing the bridge are the same as in Figure 4. (b) 3-D flux for a nearer-resonant bridge and 1-D parameters describing the bridge are the same as in Figure 5. (c) Diagram illustrating particle- and hole-transfer pathways in 3-D configuration-space.

bridge has an electron in the lower energy orbital, $V_{e-e}$ is not included, and the 3-D potential is a sum of three 1-D potentials much as the 2-D model potential was the sum of two 1-D potentials. Parts a and b of Figure 8 shows the resulting 3-D tunneling flux from donor to acceptor for nonresonant and nearer-resonant bridges, respectively, and Figure 8c illustrates the 3-D particle and hole-transfer configuration pathways. Again, we see that the nonresonant bridge flux passes solely through the particle-transfer configurations and that hole transfer only becomes significant for the nearer-resonant bridge system. Further, the only major path for the nonresonant bridge is particle transfer, but there is more than one major transfer path for the nearer-resonant bridge. In fact, there is a multiplicity of paths for the near-resonant well.

The two main transfer paths in Figure 8b for the nearer-resonant bridge represent hole- and particle-transfer paths. Of the remaining two, neither are double exchange. Scheme 5 contains a graphical depiction of the hole- and particle-transfer pathway configurations as well as the configurations involved in the two more minor transfer pathways. Both of these less significant transfer paths have configurations that resemble hole transfer and configurations that look like particle transfer. For

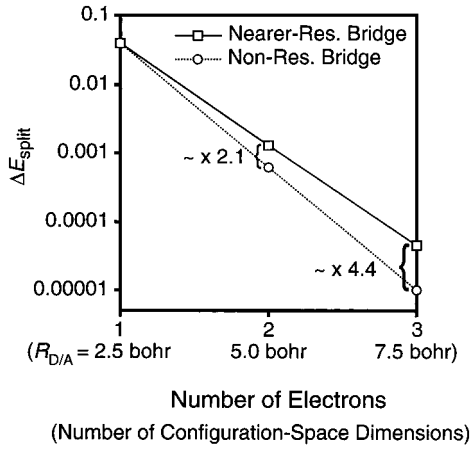


**Figure 9.** $\Delta E_{split}$ for nonresonant and nearer-resonant bridges as a function of the number of configuration-space dimensions. The 1-D model potentials used to construct 3-D nonresonant and nearer-resonant potentials are the same as those used in Figures 4 and 5, respectively. Note that as the number of electrons in the model increases, the distance between the donor and acceptor increases because bridge sites are added.

**SCHEME 5: 3-D Configuration-Space ET Pathways**

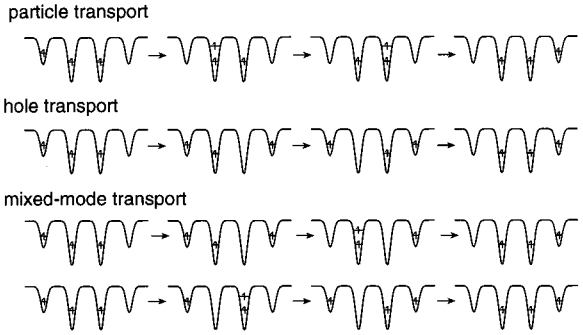


this reason, we refer to these transfer paths as mixed-mode transfer. This path multiplicity would make a larger, more complicated system very difficult to analyze in terms of particle and hole transfer by any of the popular pathway models and may also pose a challenge to the formalism used in one-electron valence atomic orbital models. However, for long-range ET by superexchange, both our model and others have indicated that the only major transfer path should be particle transfer.[26,41] Nonetheless, there is at least one recent example of a large biological electron-transfer model that is based on hole transfer.[36]

An analysis of the nearer-degenerate case shows that there are $2^n$ nearly equivalent paths for electron transfer, where $n$ is the number of bridge sites. This is borne out by the results of our model calculations. For a donor and acceptor with no intervening bridge, there is $2^0$ or one path. If one bridge site is added, there are now $2^1$ or two major transfer paths (Figure 5a and Scheme 2). Adding yet another bridge site results in $2^2$ or four major transfer paths (see Figure 8b). The enhanced rate of transfer in the resonant bridge systems can be thought of in terms of this path multiplicity. Figure 9 compares the increase in $\Delta E_{split}$ for the nearer-resonant bridge systems with several low-barrier paths compared to the nonresonant bridge systems in which there is only one low-barrier path. The observed increase in rate is within ~90% of what is predicted by the multiplicity of low-barrier paths. Also, we see that both lines in Figure 9, one for the nonresonant bridge systems and one for the nearer-resonant bridge systems, continue smoothly to the common no-bridge point (1-D).

## V. Conclusions

The results from our models support the view that many-electron effects can be reasonably small and do not greatly affect the mechanism of ET. This finding is robust in that it results from a direct comparison of our one-electron and analogous many-electron models and serves to substantiate a common practice of using one-electron models for biological ET.

We illustrate how the electronic dynamics of long-range ETs can be interpreted in a configuration-space perspective and illustrate how configuration-space models offer advantages to traditional state-space models. Perhaps the most important aspect of the model systems that we consider here is that they provide a new viewpoint in which long-range ETs are not primarily dependent on the bridge electronic states, but, in the absence of interference effects, are primarily controlled by the specifics of the bridge attractive potential. This view is complementary to, but not always conformal with, the state-based approach used in many models, even including some pathways models. Since the main focus of many long-range diabatic ET models is to accurately predict rates in large computationally intractable biological ET systems, a frequent technique is to selectively exclude states that do not affect the ET rate. This approach has been very successful when the excluded states were ancillary parts of the protein structure;[54] however, selection is frequently based on energy gap types of arguments.[5,7] This latter conventional emphasis on bridge electronic states can lead to inclusion of states that will inadequately represent the bridge attractive potential, leading to unrealistic model results. Also, many superexchange models utilize pseudopotentials. Since the form these pseudopotentials is typically based on a repulsive center, great care must be taken when choosing and implementing pseudopotential-based models. We treat this subject more fully in forthcoming work.

With respect to whether ET occurs through particle or hole transfer, we find that the mechanism is always dominated by particle transfer when the energy of the tunneling electron is far away from that of bridge eigenstates. As the energy of the electron approaches that of one bridge eigenstate, a multiplicity of transfer paths is possible and the concept of a single transfer mechanism my have limited validity for multisite bridge systems such as proteins. Further, in the context of the results herein, the concept of pure hole transfer is erroneous, and the term is simply a nomenclature to describe enhanced tunneling that occurs nearer resonance and should not be used in the context of nonresonant superexchange ET. Particle transfer then becomes a nomenclature to describe tunneling induced solely by the bridge attractive potential.

**Acknowledgment.** We gratefully acknowledge support of this work by the Welch Foundation (A-1020). M.W. thanks the U.S. Environmental Protection Agency for graduate fellowship support. The support of the Texas A&M Supercomputing Facility is also acknowledged.

## References and Notes

(1) Newton, M. D. *Chem. Rev.* **1991**, *91*, 767.
(2) Skourtis, S. S.; Beratan, D. N. *J. Biol. Inorg. Chem.* **1997**, *2*, 378.
(3) Moser, C. C.; Page, C. C.; Farid, R.; Dutton, P. L. *J. Bioenerg. Biomembr.* **1995**, *27*, 263.
(4) Larsson, S. *Bioenergetics* **1998**, *1365*, 294.
(5) Kuki, A. *Struct. Bonding (Berlin)* **1991**, *75*, 49.
(6) Hoffman, B. M.; Natan, M. J.; Nocek, J. M.; Wallin, S. A. *Struct. Bonding (Berlin)* **1991**, *75*, 85.
(7) Bertrand, P. *Struct. Bonding (Berlin)* **1991**, *75*, 3.
(8) *Protein Electron Transfer*; Bendall, D. S., Ed.; Bios Scientific: Oxford, 1996; p 300.
(9) Barbara, P. F.; Meyer, T. J.; Ratner, M. A. *J. Phys. Chem.* **1996**, *100*, 13148.
(10) *Molecular and Biomolecular Electronics*; Birge, R. R., Ed.; American Chemical Society: Washington, DC, 1994; Vol. 240, p 596.
(11) *Electron and Proton Transfer in Chemistry and Biology*; Muller, A., Ed.; Elsevier: Amsterdam, 1992; Vol. 78, p 394.
(12) Moser, C. C.; Keske, J. M.; Warncke, K.; Farid, R. S.; Dutton, P. L. *Nature* **1992**, *335*, 796.
(13) Bjerrum, M. J.; Casimiro, D. R.; Chang, I.-J.; DiBilio, A. J.; Gray, H. B.; Hill, M. G.; Langen, R.; Mines, G. A.; Skov, L. K.; Winkler, J. R.; Wuttke, D. S. *J. Bioenerg. Biomembr.* **1995**, *27*, 295.
(14) Langen, R.; Chang, I.; Germanas, J. P.; Richards, J. H.; Winkler, J. R.; Gray, H. B. *Science* **1995**, *268*, 1733.
(15) Andres, R. P.; Bein, T.; Dorogi, M.; Feng, S.; Henderson, J. I.; Kubiak, C. P.; Mahoney, W.; Osifchin, R. G.; Reifenberger, R. *Science* **1996**, *272*, 1323.
(16) Farazdel, A.; Dupuis, M.; Clementi, E.; Aviram, A. *J. Am. Chem. Soc.* **1990**, *112*, 4206.
(17) Chidsey, C. E. D. *Science* **1991**, *251*, 919.
(18) Zhang, L. Y.; Friesner, R. A.; Murphy, R. B. *J. Chem. Phys.* **1997**, *107*, 450.
(19) McConnell, H. M. *J. Chem. Phys.* **1961**, *35*, 508.
(20) Siddarth, P.; Marcus, R. A. *J. Phys. Chem.* **1993**, *97*, 13078.
(21) Stuchebrukhov, A. A.; Marcus, R. A. *J. Phys. Chem.* **1995**, *99*, 7581.
(22) Regan, J. J.; Risser, S. M.; Beratan, D. N.; Onuchic, J. N. *J. Phys. Chem.* **1993**, *97*, 13083.
(23) Lopez-Castillo, J.-M.; Jay-Gerin, J.-P. *J. Phys. Chem.* **1996**, *100*, 14289.
(24) Gray, H. B.; Winkler, J. R. *J. Electroanal. Chem.* **1997**, *438*, 43.
(25) Balabin, I. A.; Onuchic, J. N. *J. Phys. Chem.* **1996**, *100*, 11573.
(26) Kosloff, R.; Ratner, M. A. *Isr. J. Chem.* **1990**, *30*, 45.
(27) Campbell, L.; Matsen, F. A. *J. Phys. Chem.* **1996**, *100*, 1505.
(28) Sim, E.; Makri, N. *J. Phys. Chem. B* **1997**, *101*, 5446.
(29) de Andrade, P. C. P.; Onuchic, J. N. *J. Chem. Phys.* **1998**, *108*, 4292.
(30) Skourtis, S. S.; Mukamel, S. *Chem. Phys.* **1995**, *197*, 367.
(31) Kuki, A.; Wolynes, P. G. *Science* **1987**, *236*, 1647.
(32) Beratan, D. N.; Onuchic, J. N.; Hopfield, J. J. *J. Chem. Phys.* **1987**, *86*, 4488.
(33) Skourtis, S. S.; Beratan, D. N. *J. Phys. Chem. B* **1997**, *101*, 1215.
(34) Stuchebrukhov, A. A. *J. Chem. Phys.* **1997**, *107*, 6495.
(35) Stuchebrukhov, A. A. *J. Chem. Phys.* **1996**, *104*, 8424.
(36) Gruschus, J. M.; Kuki, A. *J. Phys. Chem.* **1993**, *97*, 5581.
(37) Daizadeh, I.; Gehlen, J. N.; Stuchebrukhov, A. A. *J. Chem. Phys.* **1997**, *106*, 5658.
(38) Onuchic, J. N.; Beratan, D. N.; Hopfield, J. J. *J. Phys. Chem.* **1986**, *90*, 3707.
(39) Heifets, E. N.; Daizadeh, I.; Guo, J.-X.; Stuchebrukhov, A. A. *J. Phys. Chem. A* **1998**, *102*, 2847.
(40) Kurnikov, I. V.; Zusman, L. D.; Kurnikova, M. G.; Farid, R. S.; Beratan, D. N. *J. Am. Chem. Soc.* **1997**, *119*, 5690.
(41) Stuchebrukhov, A. A. *Chem. Phys. Lett.* **1994**, *225*, 55.
(42) Cave, R. J.; Newton, M. D. *J. Chem. Phys.* **1997**, *106*, 9213.
(43) Stuchebrukhov, A. A. *Chem. Phys. Lett.* **1997**, *265*, 643.
(44) Okada, A.; Kakitani, T.; Inoue, J. *J. Phys. Chem.* **1995**, *99*, 2946.
(45) Katz, D. J.; Stuchebrukhov, A. A. *J. Chem. Phys.* **1998**, *109*, 4960.
(46) Priyadarshy, S.; Skourtis, S. S.; Risser, S. M.; Beratan, D. N. *J. Chem. Phys.* **1996**, *104*, 9473.
(47) Devault, D. *Quantum-Mechanical Tunneling in Biological Systems*, 2nd ed.; Cambridge University Press: Cambridge, 1984.
(48) Hamilton, I. P.; Light, J. C. *J. Chem. Phys.* **1986**, *84*, 306.
(49) Bransden, B. H.; Joachain, C. J. *Introduction to Quantum Mechanics*; Wiley: New York, 1989.
(50) Lopez-Castillo, J.-M.; Filali-Mouhim, A.; Nguyen, E.; Binh-Otten, V.; Jay-Gerin, J.-P. *J. Am. Chem. Soc.* **1997**, *119*, 1978.
(51) Cheong, A.; Roitberg, A. E.; Mujica, V.; Ratner, M. A. *J. Photochem. Photobiol., A* **1994**, *82*, 81.
(52) Gleiter, R.; Hoffmann, H.; Irngartinger, H.; Nixdorf, M. *Chem. Ber.* **1994**, *127*, 2215.
(53) Wells, M. C.; Lucchese, R. R. Manuscript in preparation.
(54) Gehlen, J. N.; Daizadeh, I.; Stuchebrukhov, A. A.; Marcus, R. A. *Inorg. Chim. Acta* **1996**, *243*, 271.